Hall coefficient of dilute Al-Ga and Al-Ag alloys

K. Yonemitsu
Department of Physics, Faculty of Science, Tokyo Metropolitan University, Setagayaku, Tokyo, Japan
(Received 12 February 1979)

The Hall coefficients of dilute Al-Ga and Al-Ag alloys are calculated in the intermediate magnetic-field range by path integration. The 4-OPW (orthogonalized plane wave) Fermi-surface model is used. The anisotropic electron-impurity relaxation time is included. The computational procedure of the path-integral calculation is described. The calculated Kohler plot agrees well with experiment. The effect of the anisotropy in the relaxation time on the feature of the Kohler plot of the alloys is discussed.

I. INTRODUCTION

The Hall coefficient R_H of aluminum is 10^{-11} m^3/C at the high-field limit and agrees with the theoretical value given by

$$R_H = 1/(n_h - n_e) \ ,$$

where n_h and n_e are the numbers of carriers in the second- and the third-zone Fermi sheet, respectively. R_H decreases with the decrease of the magnetic field B, changing its sign, and at the low-field limit it approaches the value given by

$$R_H = -1/Ne \ (\simeq -3.4 \times 10^{-11} \text{ m}^3/\text{C}) \ ,$$

where N is the conduction-electron concentration.[1] The phenomenon is called a high-field–low-field transition and has been studied by several authors.[2–6]

One of the most powerful tools to calculate the galvano-magnetic coefficients in the full range of the magnetic field is Schockley's tube integral[7] (or the Chambers path integral[8]). Some applied this to metals like Al,[4–6] Cd,[9,10] Cu,[11] and In,[12] and obtained results which agree well with the experimental values. Most of the calculations on Al have been made by 1-OPW (orthogonalized plane wave) approximation and on the assumption of uniform relaxation time. The simple theory predicts that a plot of R_H against B/ρ_0 (ρ_0: zero-field resistivity) is a unique curve independent of the kind of the scattering object contained in the matrix. This is the so-called Kohler rule.

Recently measurements of R_H were made on Al which contained defects or impurity atoms and it was revealed that the Kohler rule does not hold well.[13–16] In order to explain the deviation from Kohler's rule (DKR) the wave-number dependence of the relaxation time (anisotropic relaxation time) must be taken into account. Attempts to explain DKR in terms of the anisotropic relaxation time and the simplified Fermi-surface model have been made by several authors.[3,13] Kesternich *et al.*[3] have divided the Fermi surface of Al into three parts and assuming that each part has its individual mean free path have explained qualitatively the occurrence of a minimum in the Kohler plot of Al in which defects were introduced.

To obtain a more quantitative agreement between experiment and the calculation without any adjustable parameters, we must do the calculation on a more realistic model of the Fermi surface, taking the more correct anisotropy of the relaxation time into account. In the low-field limit we have shown that our exact calculation about the 4-OPW Fermi surface can explain the measured R_H of the dilute Al alloys fairly well.[17] In the calculation the scattering potential of the model pseudopotential was used, and the relaxation time was obtained by iterative solution of Boltzmann's equation. In the present work we will describe the path-integral result about Al-Ga and Al-Ag alloys by a 4-OPW approximation. We select the Al-Ga alloy because it has several distinctive features: it has a large positive R_H value at the low-field limit [$R_H = (4.0 \text{ or } 6.4) \times 10^{-11}$ m^3/C][15,16] and there is a minimum in Kohler's plot of the alloy. On the other hand the low-field limit of the R_H value of the Al-Ag alloy is small and negative and its Kohler's plot is monotonic. The main object of the present calculation is to see whether such a difference of Kohler's plot between Al-Ga and Al-Ag can be explained in terms of the difference of the anisotropy of the relaxation time between them.

The anisotropic relaxation times which were calculated in our previous work[17] are used here again. The direction of the magnetic field is selected parallel to the [110] axis. The selection of the direction is optional. Since these alloys have cubic symmetry, we will get a similar result if we select another direction of the magnetic field.

II. THEORY AND COMPUTATIONAL PROCEDURE

A. Path-integral equation

We have briefly mentioned the path-integral procedure by 4-OPW approximation when the relaxation time τ is constant before.[18] Here we will give the more detailed description when τ is a function of the wave number k, supplementing several points that we have left out before.

We start our computation from the Chambers equation,[8]

$$\sigma_{ij}=-\left(\frac{e^2}{4\pi^3}\right)\int v_i(k)\left(\frac{\partial f_0}{\partial E}\right)d\vec{k}\int_{-\infty}^{t}dt'\,v_j(t')\times\exp\left[-\int_{t'}^{t}\frac{du}{\tau(u)}\right], \tag{2.1}$$

where $v_i(k)$ and $v_j(t')$ are i and j components of the velocity, f_0 is the equilibrium distribution function, and t, t', and u are time variables. Hereafter the wave number is expressed by the unit of $2\pi/a$ where a is the lattice parameter of Al ($a=4.04$ Å) and the unit of energy and potential is $(\hbar^2/2m)(2\pi/a)^2=0.6777$ Ry. We take the z axis parallel to the magnetic field B and rewrite Eq. (2.1) in a Cartesian coordinate (see Appendix)

$$\sigma_{ij}=\left(\frac{2e}{a^3}\right)\left(\frac{1}{B}\right)\sum_{\alpha}\int dk_z\,(1-e^{-1/\omega\bar{\tau}_\alpha})^{-1}\times I_i^k I_j^{k'}e^{-\omega^{-1}T(k,k')}, \tag{2.2}$$

$$I_i^k=\oint\frac{dk_m\,v_i(k)}{|v_n(k)|}, \tag{2.3}$$

$$T(k,k')=\int_{k'}^{k}\frac{dk_m''}{\tau(k'')|v_n(k'')|}, \tag{2.4}$$

$$\bar{\tau}_\alpha(k_z)^{-1}=\oint\frac{dk_m}{\tau(k)|v_n(k)|}, \tag{2.5}$$

where $\omega=eB/2m$ and α represents the type of orbits. The suffix m represents x (or y) when k_x (or k_y) is selected as the independent variable and the suffix n represents y (or x) when k_y (or k_x) is selected as the dependent variable. As for the selection of the variables, we will expatiate on it in Sec. II B. For convenience sake we call the integrals in Eq. (2.2) by the following terms:

$\int dk_z$: "k_z integral" ;

I_i^k: "k integral" ;

$I_j^{k'}$: "k' integral" ;

and

$T(k,k')$: "τ integral" .

The relaxation time $\tau(\vec{k})$ is given by

$$\begin{aligned}\tau(\vec{k})=&C_0^i\left(3-\sum\cos\tfrac{1}{2}ak_y\cos\tfrac{1}{2}ak_z\right)+C_{200}^i\left(3-\sum\cos ak_x\right)\\&+C_{211}^i\left(3-\sum\cos ak_x\cos\tfrac{1}{2}ak_y\cos\tfrac{1}{2}ak_z\right)+C_{220}^i\left(3-\sum\cos ak_y\cos ak_z\right)\\&+C_{310}^i\left(6-\sum\cos\tfrac{3}{2}ak_x\cos\tfrac{1}{2}ak_y-\sum\cos\tfrac{3}{2}ak_y\cos\tfrac{1}{2}ak_x\right)+C_{222}^i\left(1-\sum\cos ak_x\cos ak_y\cos ak_z\right)\\&+C_{321}^i\left(6-\sum\cos\tfrac{3}{2}ak_x\cos ak_y\cos\tfrac{1}{2}ak_z-\sum\cos\tfrac{3}{2}ak_z\cos ak_y\cos\tfrac{1}{2}ak_x\right),\end{aligned} \tag{2.6}$$

where the superfix i is II for the second-zone Fermi sheet and is III for the third zone. The Fourier coefficients C_0^i, C_{200}^i, . . . , are determined by the least-square fit of Eq. (2.6) to the relaxation times which we calculated about 131 points of $\frac{1}{48}$ of the Fermi surface of Al-Ga (1 at.%) and Al-Ag (1 at.%) alloys.[17] They are given in Table I. The relaxation times along the (110) section of the second-zone Fermi sheet are shown in Fig. 1.

The computation consists of three main steps: the

TABLE I. Fourier expansion coefficients of the local relaxation time $\tau(k)$ of Al-Ga and Al-Ag alloys.

Al-Ga	C_0	C_{200}	C_{211}	C_{220}	C_{310}	C_{222}	C_{321}
zone							
II(10^{-13}s)	−10.17	−3.77	+1.67	+4.82	+1.03	+4.46	+3.41
III (10^{-12} s)	−17.24	−2.62	+7.53	+5.40	+2.50	+4.37	+2.30
Al-Ag	C_0	C_{200}	C_{211}	C_{220}	C_{310}	C_{222}	C_{321}
zone							
II (10^{-14} s)	−3.30	−1.21	+1.11	+1.74	+0.39	+1.11	+0.92
III (10^{-13} s)	+9.57	+7.08	−5.41	−8.00	−0.25	−0.37	−1.70

first is the tracing step where we trace an orbit while computing $v_j(\vec{k})$ and $T(k,k')$; the second is the orbital integration step where k and k' integrals in Eq. (2.2) are made; the third one is the k_z-integration step. In Secs. II B–II E we will give a full explanation of the first and the second steps.

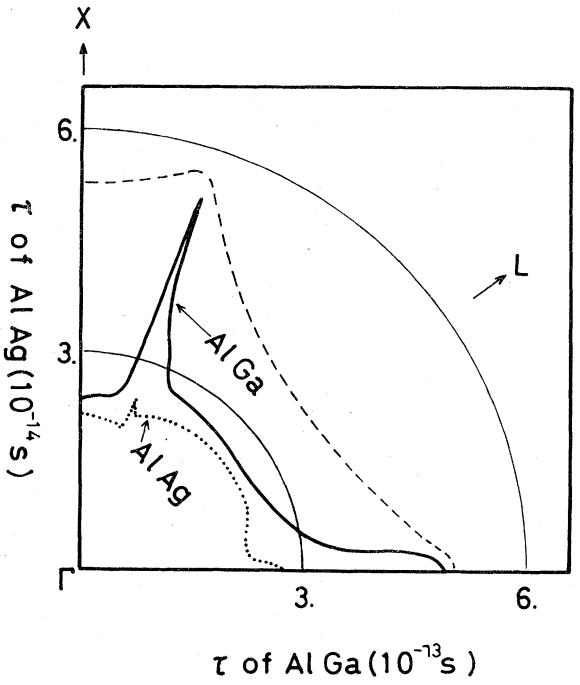

FIG. 1. Local relaxation time of Al-Ga and Al-Ag on the [110] central orbit of the second zone Fermi sheet. The orbit is shown by a dashed curve. L shows [111] direction.

B. Tracing step

The wave-number space is divided into tetrahedra and apices of which are $\vec{G}_0=\{0,0,0\}$, $\vec{G}_1=\{1,1,1\}$, $\vec{G}_2=\{1,-1,1\}$, and $\vec{G}_3=\{0,0,2\}$. In one tetrahedron, the 4-OPW Fermi surface is given by an equation

$$S(k_x,k_y,k_z,E_F)=0 \ , \tag{2.7}$$

where S is the determinant

$$S=\begin{vmatrix} \vec{k}^2-E & V_{111} & V_{111} & V_{002} \\ V_{111} & |\vec{k}-\vec{G}_1|^2-E & V_{002} & V_{111} \\ V_{111} & V_{002} & |\vec{k}-\vec{G}_2|^2-E & V_{111} \\ V_{002} & V_{111} & V_{111} & |\vec{k}-\vec{G}_3|^2-E \end{vmatrix} . \tag{2.8}$$

In these equations V_{111} and V_{002} are the Fourier components of the pseudopotential of Al at $\vec{G}_1$ and $\vec{G}_3$; E_F is the Fermi energy. The parameters determined by Ashcroft are used in the above; consequently $V_{111}=0.0179$ Ry, $V_{002}=0.0562$ Ry, and $E_F=0.85605$ Ry.[19]

The tracing program is called LOOPER. To start LOOPER we must give the starting point coordinates (k_x,k_y,k_z), in which k_z is fixed to some constant value. One of k_x and k_y is assigned as the independent variable, which is denoted as k_m; the other is assigned as the dependent variable which is denoted as k_n. The value of k_m must be given exactly but the value of k_n is of course approximate. As the initial data we must also give the values of G_i $(i=0,1,2,3)$, the value of a step interval Δk_m which is usually taken to be 0.01, and the sign of $\partial E/\partial k_n$.

The LOOPER has the following functions: (i) The LOOPER solves Eq. (2.7) by Newton's approximation to get a more accurate value of k_n by which

$|S| < 10^{-10}$. (ii) Starting from the initial point, it, so to speak, gropes its way. At every point (which is numbered as l) it computes $\partial S/\partial k_i$ (i represents x, y, or z) and $\partial S/\partial E$, from which $dk_n/dk_m = -(\partial S/\partial k_m)/(\partial S/\partial k_n)$ and $v_i(\vec{k}) = -(\partial S/\partial k_i)/(\partial S/\partial E)$ are computed. Now we adapt the notation by which the wave number, the velocity, relaxation time, k and k' integrals at l th point or l'th point are denoted as $k(l)$, $v(l)$, $\tau(l)$, I_i^l, and $I_j^{l'}$. The τ integral from the starting point (where $l=1$) to the l th point is also denoted as $T(l,1)$. (iii) To go to the $(l+1)$th point from the l th point, $k_m(l+1)$, and $k_n(l+1)$ are given by

$$k_m(l+1) = k_m(l) + \Delta k_m$$

and

$$k_n(l+1) = k_n(l) + \left(\frac{dk_n}{dk_m}\right)_l \Delta k_m \quad .$$

(iv) The LOOPER always checks whether $\partial E/\partial k_n$ has the correct sign. This is necessary for the LOOPER not to lose its correct orbit. (v) It checks whether $|dk_n/dk_m| < 1$. If $|dk_n/dk_m| > 1$ it changes the role of independent and dependent variables. (vi) The LOOPER computes the radius of curvature k_{rc} of the orbit at every point and when k_{rc} becomes very small, the step interval Δk_m is automatically shortened. (vii) While tracing an orbit the LOOPER computes the τ integral $T(l,1)$. The data of $v_i(l)$, $T(l,1)$, and other information which is necessary to make the next computation step are written down in a file on a magnetic disk. (viii) When the LOOPER steps out from the original tetrahedron, it automatically selects the new $\vec{G}_i$ values which give the coordinates of apices of the new tetrahedron in which the LOOPER is located. (ix) When the LOOPER comes back after N_s steps to near the starting point ($l=1$), it stops.

C. Orbital-integration step

The program called PATH works in this step. It reads N_s data of $v_i(l)$, $T(l,1)$, and other necessary information from the file made by the LOOPER. We will show how the integrand of the k' integral at point l on an orbit is calculated. It takes another point l' where l's are $l, l-1, l-2, \ldots, 2, 1, N_s, \ldots, l+1, l$. PATH also knows the values of the velocity $v_j(l')$. The exponential factor is computed by

$$\exp\{-\omega^{-1}[T(l',1) - T(l,1)]\} \quad .$$

Thus the necessary data are all known. Varying l' from l to N_s and from N_s to l, the k' integral is achieved numerically.

D. Conductivity tensor and the Hall coefficient

In the present direction of the magnetic field, the σ tensor is given by

$$\sigma = \begin{pmatrix} \sigma_{11} & \sigma_{12} & 0 \\ \sigma_{21} & \sigma_{22} & 0 \\ 0 & 0 & \sigma_{33} \end{pmatrix} , \tag{2.9}$$

where $\sigma_{12} = -\sigma_{21}$ and $\sigma_{11} = \sigma_{22}$. The equalities are used to check the error of the computation, which is of order of 1%. The Hall coefficient R_H is given by

$$R_H = R_H^{II} + R_H^{III} = (\sigma_{21}^{II} + \sigma_{21}^{III})/\Delta B \quad , \tag{2.10}$$

where superfixes II and III represent the second- and third-zone contributions, respectively, and

$$\Delta = \sigma_{11}\sigma_{22} - \sigma_{21}\sigma_{12} = \sigma_{22}^2 + \sigma_{21}^2 \quad . \tag{2.11}$$

E. Types of orbits

There are six types of orbits when $\vec{B} \parallel [110]$. They are denoted as a, a' (second zone); b, c, d, and e (third zone). The typical orbits of each group are shown in Figs. 2(a) and 2(b). The numbers of orbits computed are: 49 a and a' orbits, 16 b orbits, 27 c orbits, 17 d orbits, and 9 e orbits. In the computation of σ tensor, we can make use of the symmetry of orbits to save computation time.

We suggest that $\bar{\tau}_\alpha(k_z)$ defined by Eq. (2.5) be called "orbital relaxation time of the α orbit" and show it in Figs. 3(a) and 3(b). The orbital relaxation time is closely related to the high-field–intermediate-field transition of an orbit. From orbit to orbit $\bar{\tau}_\alpha(k_z)$ varies, which will be referred to as the "anisotropy of the orbital relaxation time". To avoid confusion we call the relaxation time defined at point $\vec{k}$ by Eq. (2.6) as "local relaxation time". On an orbit the local relaxation time is not uniform, which will be referred to as the "anisotropy of the local relaxation time". We also define $\bar{\tau}_0 = \bar{\tau}_\alpha(0)$, the orbital relaxation time of the a orbit at $k_z = 0$, and measure ω by the unit of $\bar{\tau}_0^{-1}$. We have made computations for these values of $\omega\bar{\tau}_0$ for which $\omega\bar{\tau}_0 = 1.94$, 0.194, 0.0642, 0.0194, and 0.00642 for Al-Ga and $\omega\bar{\tau}_0 = 2.0$, 0.2, 0.064, 0.002, and 0.0064 for Al-Ag.

III. RESULTS AND DISCUSSION

The final results are shown in Fig. 4 where large open circles are for Al-Ga and large open squares are for Al-Ag. In the figure, the experimental values are also shown for Al-Ga (○,+), for Al-Ag (×), and for pure Al(●). The zero-field resistivity ρ_0 in the horizontal axis has been calculated for the relaxation

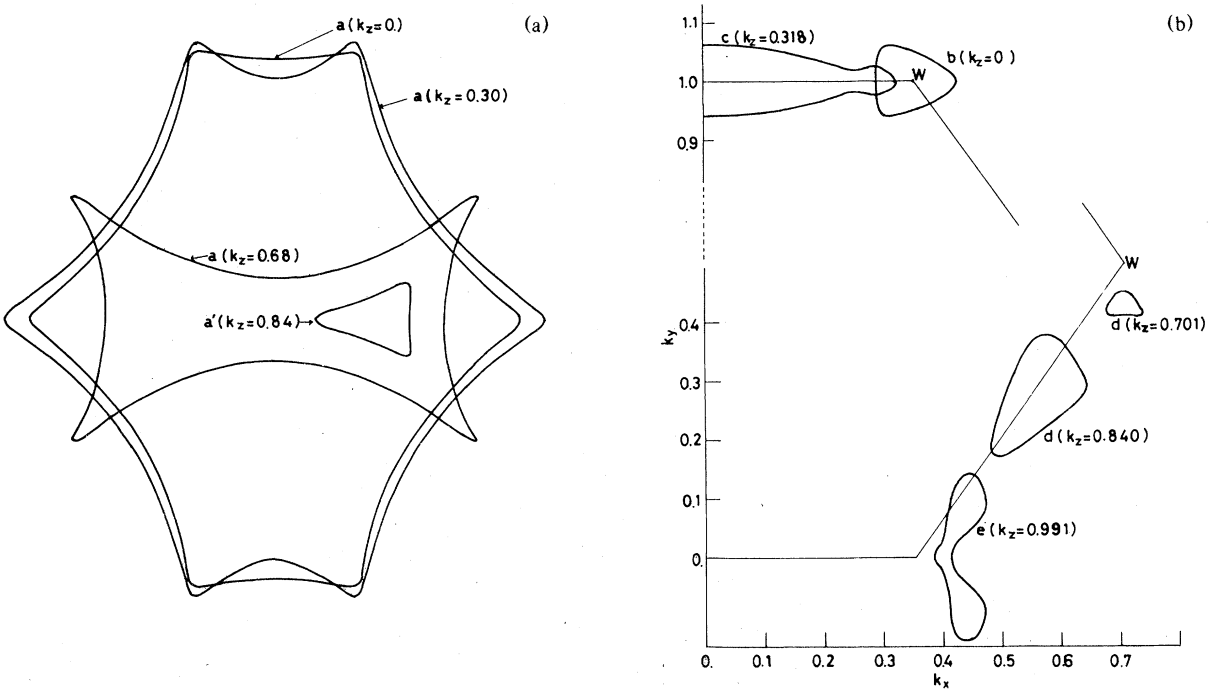

FIG. 2. Typical cyclotron orbits when the magnetic field is parallel to the [110] axis. (a) The second-zone orbits which are denoted as a and a'. (b) The third-zone orbits which are denoted as b, c, d, and e. The Brillouin-zone boundary is shown by thin lines. W's are corners of fcc Brillouin zone.

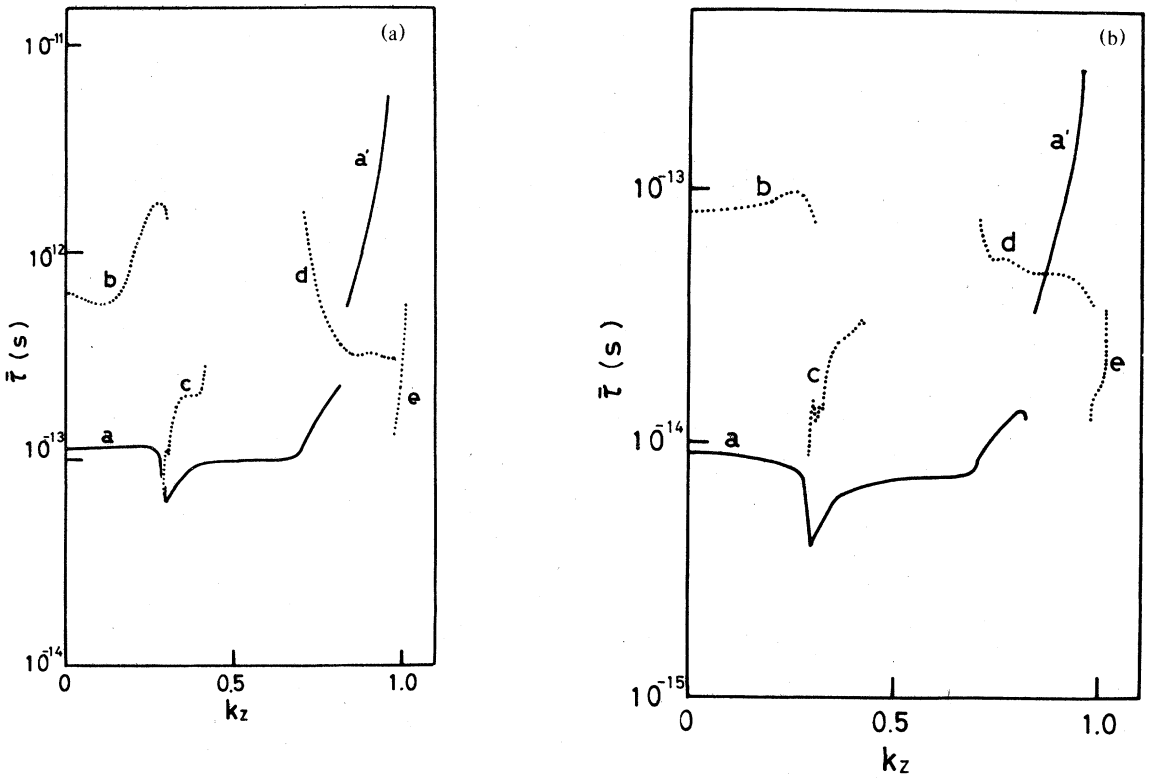

FIG. 3. Orbital relaxation time of every orbit as function of k_z. The solid curves are for the second zone and the dotted curves are for the third zone; (a) for Al-Ga and (b) for Al-Ag.

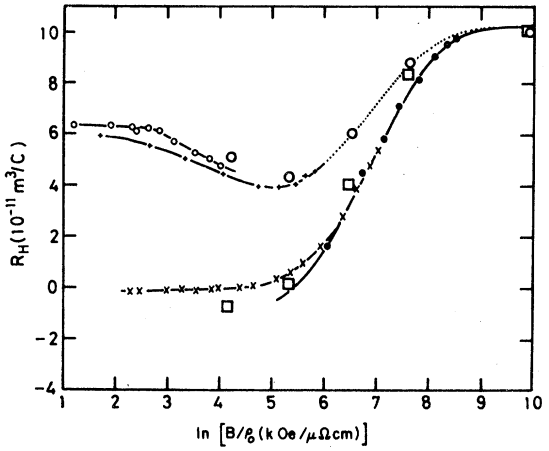

FIG. 4. Kohler's plot of R_H of Al and Al alloys. ○, calculated values of Al-Ga; □, calculated values of Al-Ag; ●, experimental values of pure Al; o, experimental values of Al-Ga; +, experimental values of very dilute Al-Ga alloys. The difference of + data from o data is due to the residual impurity in the solvent (see Ref. 16). ×, experimental values of Al-Ag.

times given by Eq. (2.6), by means of the computational program which was reported in the previous paper.[17] $\rho_0 = 0.094\ \mu\Omega$ cm/at.% for Al-Ga and $\rho_0 = 1.23\ \mu\Omega$ cm/at.% for Al-Ag. The results of the computation agree quite well with the experimental curves. The individual contributions R_H^{II} and R_H^{III} are shown in Fig. 5, in which they are plotted against $\omega\bar{\tau}_0$. From the figure we see that R_H is nearly equal to the high-field limiting value at $\omega\bar{\tau}_0 \geqslant 1$. When $\omega\bar{\tau}_0 \geqslant 1$, most electrons revolve around their orbits more than once before they decay to $1/e$. Electrons go through all the variations of $v(\vec{k})$ or $\tau(\vec{k})$ on their orbits, and the resultant σ_{ij} or R_H does not depend on the anisotropy of $\vec{v}(\vec{k})$ or $\tau(\vec{k})$.

To explain the reason for the difference of the field dependence of R_H between two alloys in the range $\omega\tau_0 < 0.1$, it is convenient to rewrite Eq. (2.10)

$$R_H = \frac{\sigma_{21}^{II}/\sigma_0^2 B + \sigma_{21}^{III}/\sigma_0^2 B}{\Delta/\sigma_0^2}\ , \tag{3.1}$$

where $\sigma_0 = 1/\rho_0$.

In Figs. 6(a) and 6(b) we show the terms in the numerator $\sigma_{21}^i/\sigma_0^2 B$ (i = II,III) and the denominator Δ/σ_0^2 for both alloys, in the case of Al-Ga by dashed curves and in the case of Al-Ag by dotted curves. Since the denominators Δ/σ_0^2 of both alloys are nearly equal, it follows that the difference of the field dependence of R_H between the two alloys in the range comes from the difference of their numerators. The quantity $\sigma_{21}^i/\sigma_0^2 B$ tends to a constant in the low-field condition, and

$$\lim_{B\to 0}(\sigma_{21}^i/\sigma_0^2 B) = \lim_{B\to 0} R_H^i\ .$$

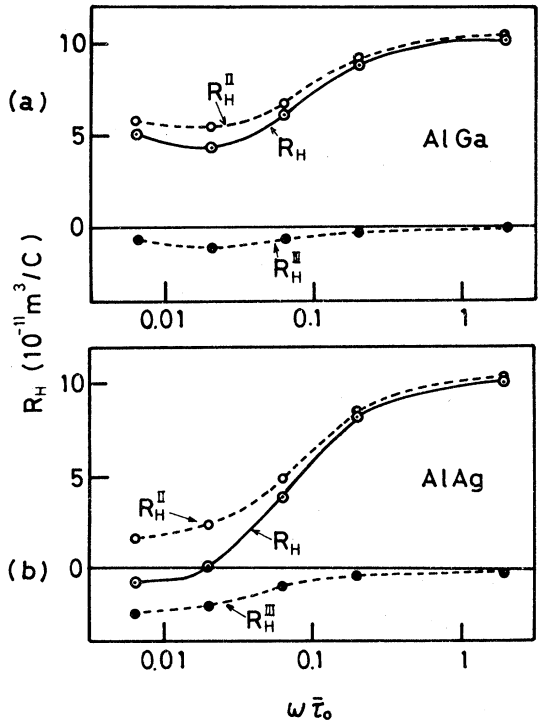

FIG. 5. Calculated values of R_H against $\omega\bar{\tau}_0$. (a) Al-Ga, (b) Al-Ag. ○, the second-zone contribution, R_H^{II}. ●, the third-zone contribution, R_H^{III}. ⊙, the resultant $R_H(=R_H^{II}+R_H^{III})$.

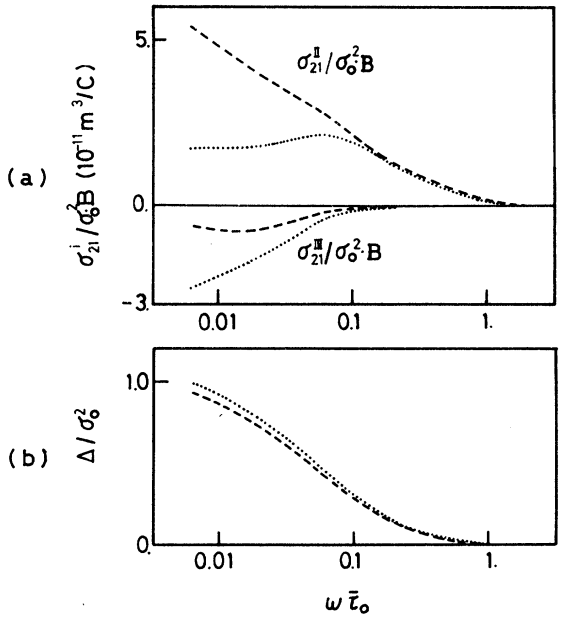

FIG. 6. (a) Two terms in the numerator of Eq. (3.1), $\sigma_{21}^{II}/\sigma_0^2 B$ and $\sigma_{21}^{III}/\sigma_0^2 B$ against $\omega\bar{\tau}_0$. (b) The denominator of Eq. (3.1). In (a) and (b), the dashed curves are for Al-Ga and the dotted curves are for Al-Ag.

Since $\sigma_{21}^{II}/\sigma_0^2 B$ of Al-Ag and $\sigma_{21}^{III}/\sigma_0^2 B$ of Al-Ga are nearly constant in the range $\omega\bar{\tau}_0 < 0.06$, we can conclude that the second-zone Fermi sheet of Al-Ag and the third-zone Fermi sheet of Al-Ga are nearly in the low-field condition in the range. This is also to be seen from Figs. 7 and 8 where we plot the $(d\sigma_{21}^{\alpha}/dk_z)/B$ against k_z for orbits of the second zone and the third zone of both alloys. The dotted curves are for $\omega\bar{\tau}_0 = 0.064$, the dashed curves are for $\omega\bar{\tau}_0 = 0.02$ and the solid curves are for $\omega\bar{\tau}_0 = 0.0064$. If any two curves of a Fermi sheet for two values of $\omega\bar{\tau}_0$, say $\omega\bar{\tau}_{01}$ and $\omega\bar{\tau}_{02}$, coincide or nearly coincide, we can safely say that the sheet attains the low-field condition in the range between $\omega\bar{\tau}_{01}$ and $\omega\bar{\tau}_{02}$. It is also to be noted that if a group of orbits attains the low-field condition, its $(d\sigma_{21}^{\alpha}/dk_z)/B$ curve shows a kind of structure which reflects the anisotropy of the orbital relaxation time $\bar{\tau}_{\alpha}(k_z)$, while the curve is smooth if it is in the intermediate-field condition. According to the discussion above with the examination of Figs. 7 and 8, for Al-Ga, most of the *b*, *c*, *d*, and *e* orbits are nearly in the low-field condition in the range of $\omega\bar{\tau}_0 < 0.02$, while most of the *a* orbits are still in the intermediate-field condition. For Al-Ag, however, *a* orbits are nearly in the low-field condition, while *b*, *d*, and *e* orbits are still in the intermediate-field condition.

The behavior of an orbit in the lower $\omega\bar{\tau}_0$ region is largely affected by the anisotropy of the local relaxation time $\tau(\vec{k})$ on the orbit. Under the situation in which the electronic velocity varies widely in a life of an electron, the contribution of the electron to the conductivity is much dependent on the magnetic-field strength. As an example, we can consider electrons excited at a corner of the *a* orbit of Al-Ga. Since $\tau(\vec{k})$ is markedly long at the corner, $\vec{v}(\vec{k})$ varies abruptly there; the integrand of the k' integral changes its sign in the lives of the electrons in the field as low as $\omega\bar{\tau}_0 = 0.02$. Accordingly at one time in their lives they make a negative contribution to σ_{21}

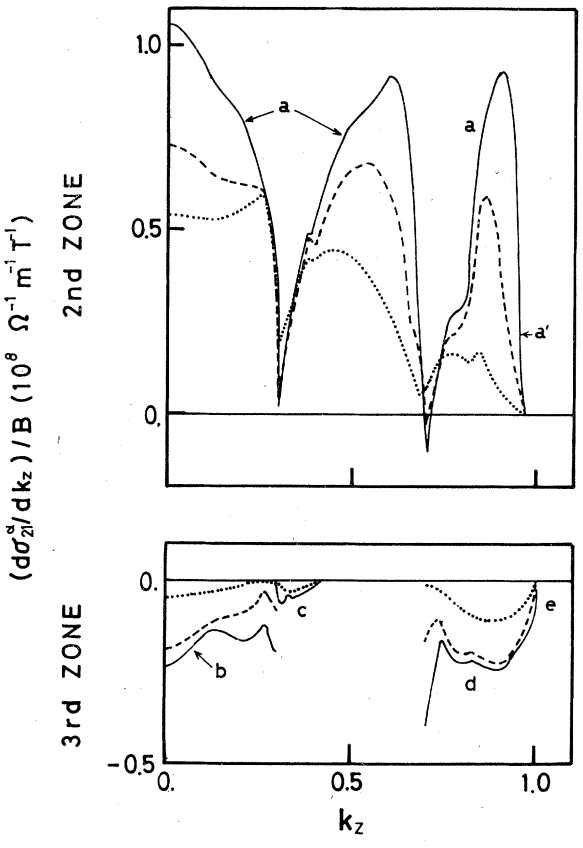

FIG. 7. $(d\sigma_{21}^{\alpha}/dk_z)/B$ against k_z for Al-Ga, where the superscript represents the type of the orbits. The dotted curves are for $\omega\bar{\tau}_0 = 0.0642$, the dashed curves are for $\omega\bar{\tau}_0 = 0.0194$ and the solid curves are for $\omega\bar{\tau}_0 = 0.00642$.

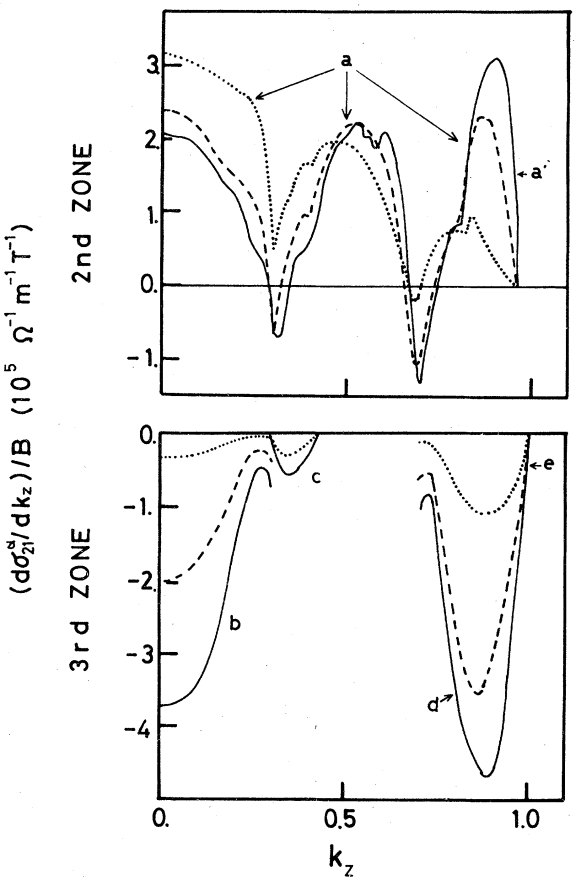

FIG. 8. $(d\sigma_{21}^{\alpha}/dk_z)/B$ against k_z for Al-Ag, where the superscript represents the type of the orbits. The dotted curves are for $\omega\bar{\tau}_0 = 0.064$, the dashed curves are for $\omega\bar{\tau}_0 = 0.02$, and the solid curves are for $\omega\bar{\tau}_0 = 0.0064$.

and at the other time they make a positive contribution. With decrease of $\omega\bar{\tau}_0$ the negative contribution decreases and therefore $\sigma_{21}^{II}/\sigma_0^2 B$ increases as shown if Fig. 6(a). The increment is nearly cancelled by the increment of the denominator and we can find only a slight minimum in the curve of R_H^{II} of Fig. 5(a).

The occurrence of the minimum in the curve of R_H^{III} of Al-Ga in Fig. 5(a) is understood in terms of the behavior of the third-zone sheet of the alloy: in the range $\sigma_{21}^{III}/\sigma_0^2 B$ is nearly constant, but with decrease of $\omega\bar{\tau}_0$ the denominator Δ/σ_0^2 goes on increasing which results in the minimum. The minimum is superposed with the minimum of R_H^{II} and the minimum of the resultant R_H curve becomes conspicuous. In Al-Ag the a orbits attain the low-field condition in the range since $\tau(\vec{k})$ is more isotropic and the electrons at the corner transit to the low field along with the electrons at the other parts of the orbit. Thus $\sigma_{21}^{II}/\sigma_0^2 B$ is nearly constant but $\sigma_{21}^{III}/\sigma_0^2 B$ still goes on decreasing since most of the third-zone orbits are still in the intermediate-field condition, which results in the monotonic R_H curve of Al-Ag.

In this calculation, we have neglected the dependence of the relaxation time on the magnetic-field strength. The present result shows that at least for the Hall coefficient, we can explain the DKR by the anisotropy of the zero-field relaxation time.

From the above we conclude that the path integral is a quite efficacious device in the calculation of the galvano-magnetic coefficient if we use a realistic Fermi-surface model taking the proper anisotropic relaxation time into account.

The programs LOOPER and PATH are available from the author.

ACKNOWLEDGMENT

The author wishes to thank Dr. K. Takano, Dr. I. Shiozaki, Dr. H. Sato, and Dr. I. Sakamoto for valuable discussions. He also wishes to thank Professor T. Matsunami for his help with the English.

APPENDIX

If there are no open orbits, Eq. (2.1) is rewritten

$$\sigma_{ij} = -\frac{e^2}{4\pi^3}\int d\vec{k}\, v_i(\vec{k})\frac{\partial f_0}{\partial E}\left[1-\exp\left(-\oint\frac{du}{\tau(u)}\right)\right]^{-1}\cdot \times\oint dt'\, v_j(t')\exp\left(-\int_{t'}^{t}\frac{du}{\tau(u)}\right) . \quad \text{(A1)}$$

The volume element $d\vec{k}$ in the wave-number space is given by

$$d\vec{k} = \frac{dk_z\, dk_T\, dE}{|\nabla_\perp E|} , \quad \text{(A2)}$$

where dk_T is the line element along a path and $\nabla_\perp E$ is the projection of $\nabla_k E$ in the orbital plane. The time variables are rewritten

$$dt' = \left(\frac{\hbar^2}{eB}\right)\left(\frac{dk_T'}{|\nabla_\perp' E|}\right)$$

and

$$du = \left(\frac{\hbar^2}{eB}\right)\left(\frac{dk_T''}{|\nabla'' E|}\right) . \quad \text{(A3)}$$

We substitute Eqs. (A2) and (A3) into Eq. (A1) and integrate with E to obtain

$$\sigma_{ij} = \frac{e}{4\pi^3}\frac{\hbar^2}{B}\sum_\alpha\int dk_z\left[1-\exp\left(-\oint\frac{du}{\tau(u)}\right)\right]^{-1}\oint v_i(\vec{k})\frac{dk_T}{|\nabla_\perp E|}\oint v_j(\vec{k}')\frac{dk_T'}{|\nabla_\perp E|}\exp\left[-\left(\frac{\hbar^2}{eB}\right)\int_{k'}^{k}\frac{dk_T''}{\tau(\vec{k}'')|\nabla_\perp'' E|}\right] . \quad \text{(A4)}$$

We express k and E in units of $2\pi/a$ and $(\hbar^2/2m)(2\pi/a)^2$ respectively and rewrite Eq. (A4)

$$\sigma_{ij} = \left(\frac{2e}{a^3}\right)\left(\frac{1}{B}\right)\sum_\alpha\int dk_z\left[1-\exp\left(-\omega^{-1}\int\frac{dk_T''}{\tau(\vec{k}'')|\nabla_\perp'' E|}\right)\right]^{-1}\left(\oint\frac{dk_T\nabla_i E}{|\nabla_\perp E|}\right)\left(\oint\frac{dk_T'\nabla_j' E}{|\nabla_\perp' E|}\right) \times\exp\left(-\omega^{-1}\int_{k'}^{k}\frac{dk_T''}{\tau(\vec{k}'')|\nabla_\perp'' E|}\right) . \quad \text{(A5)}$$

We introduce the integral operators

$$I_j^k = \oint\frac{dk_T\nabla_j E}{|\nabla_\perp E|} \quad \text{(A6)}$$

and

$$T(k,k') = \int_{k'}^{k}\frac{dk_T''}{\tau(k'')|\nabla_\perp'' E|} . \quad \text{(A7)}$$

Equation (A6) is rewritten

$$\oint \frac{dk_T \nabla_j E}{|\nabla_\perp E|} = \oint (dk_x^2 + dk_y^2)^{1/2} \nabla_j E \Big/ \left[\left(\frac{\partial E}{\partial k_x} \right)^2 + \left(\frac{\partial E}{\partial k_y} \right)^2 \right]^{1/2}$$

$$= \oint dk_x \left[1 + \left(\frac{dk_y}{dk_x} \right)^2 \right]^{1/2} \nabla_j E \Big/ \left(\left| \frac{\partial E}{\partial k_y} \right| \left\{ 1 + \left[\left(\frac{\partial E}{\partial k_x} \right) \Big/ \left(\frac{\partial E}{\partial k_y} \right) \right]^2 \right\}^{1/2} \right)$$

$$= \oint dk_x \left[1 + \left(\frac{dk_y}{dk_x} \right)^2 \right]^{1/2} \nabla_j E \Big/ |v_y| \left[1 + \left(\frac{dk_y}{dk_x} \right)^2 \right]^{1/2}$$

$$= \oint dk_x \, \nabla_j E / |v_y| \ , \tag{A8}$$

and similarly

$$= \oint dk_y \nabla_j E / |v_x| \ . \tag{A9}$$

The Eq. (A7) is also rewritten similarly. The rewritten operators are substituted into Eq. (A5) and we obtain Eq. (2.2).

---

[1]K. Førsvoll and I. Holwech, Philos. Mag. 10, 921 (1964).
[2]N. W. Ashcroft, Phys. Kondens. Mater. 9, 45 (1969).
[3]W. Kesternich, H. Ullmaier, and W. Schilling, J. Phys. F 6, 1867 (1976).
[4]J. Feder and J. Lothe, Philos. Mag. 12, 107 (1965).
[5]R. J. Douglas and W. R. Datars, Can. J. Phys. 51, 1770 (1973).
[6]N. C. Banik and A. W. Overhauser, Phys. Rev. B 18, 1521 (1978).
[7]W. Shockley, Phys. Rev. 79, 191 (1950).
[8]R. G. Chambers, Proc. R. Soc. London Sect. A 202, 378 (1950).
[9]J. E. A. Alderson, C. M. Hurd, and S. P. McAlister, Can. J. Phys. 54, 1866 (1976).
[10]C. M. Hurd, J. E. A. Alderson, and S. P. McAlister, Phys. Rev. B 14, 395 (1976).
[11]C. M. Hurd and S. P. McAlister, J. Phys. F 7, 969 (1977).
[12]R. J. Douglas and W. R. Datars, Can. J. Phys. 52, 714 (1974).
[13]K. Böning, K. Pfändner, P. Rosner, and M. Schlüter, J. Phys. F 5, 1176 (1975).
[14]W. Kesternich, H. Ullmaier, and W. Schilling, Philos. Mag. 31, 471 (1975).
[15]C. Papastaikoudis, E. Rocoffylou, W. Tselfes, and K. Chountas, Z. Phys. B 25, 131 (1976).
[16]H. Sato, T. Babauchi, and K. Yonemitsu, Phys. Status Solidi B 89, 571 (1978).
[17]K. Yonemitsu, K. Takano, and T. Matsuda, Phys. Status Solidi B 88, 273 (1978).
[18]H. Sato and K. Yonemitsu, J. Phys. F 8, 659 (1978).
[19]N. W. Ashcroft, Philos. Mag. 8, 2055 (1963).